nature physics

ARTICLES

PUBLISHED ONLINE: 2 DECEMBER 2012 | DOI: 10.1038/NPHYS2494

Supercollision cooling in undoped graphene

A. C. Betz[1†], S. H. Jhang[1†], E. Pallecchi[1,2], R. Ferreira[1], G. Fève[1], J-M. Berroir[1] and B. Plaçais[1*]

Carrier mobility in solids is generally limited by electron-impurity or electron–phonon scattering, depending on the most frequently occurring event. Three-body collisions between carriers and both phonons and impurities are rare; they are denoted supercollisions. Elusive in electronic transport they should emerge in relaxation processes as they allow for larger energy transfers. This is the case in undoped graphene, where the small Fermi surface drastically restricts the allowed phonon energy in ordinary collisions. Using electrical heating and sensitive noise thermometry we report on supercollision cooling in diffusive monolayer graphene. At low carrier density and high phonon temperature the Joule power P obeys a $P \propto T_e^3$ law as a function of electronic temperature T_e. It overrules the linear law expected for ordinary collisions which has recently been observed in resistivity measurements. The cubic law is characteristic of supercollisions and departs from the T_e^4 dependence recently reported for doped graphene below the Bloch–Grüneisen temperature. These supercollisions are important for applications of graphene in bolometry and photo-detection.

Understanding how two-dimensional (2D) electrons in graphene relax their energy to the lattice is not only a central problem in condensed matter physics but also an important issue in the design of graphene devices[1,2]. Owing to the large optical phonon energy of $\Omega \approx 200$ meV in graphene, the emission of acoustic phonons is the only efficient cooling pathway for hot electrons below the energy Ω. Unlike conventional metals with large Fermi surfaces, where the Debye temperature sets the boundary between high- and low-temperature behaviour in the electron–phonon interaction, a new characteristic temperature arises in graphene, the Bloch–Grüneisen temperature (T_{BG}). It results from the small Fermi surface in graphene and is defined by the maximum phonon wave vector $q_{max} = 2k_F$ where k_F is the Fermi wave vector (Fig. 1b). Above T_{BG}, only a fraction of acoustic phonons with wave vector $q \leq 2k_F$ can scatter off electrons. This phase space restriction leads to the crossover behaviour of electron–phonon resistivity between high-temperature $\rho(T) \propto T$ and low-temperature $\rho(T) \propto T^4$ dependence[3]. It also imposes a significant constraint on the cooling of hot electrons; the energy dissipated by acoustic phonons cannot exceed $k_B T_{BG}$ per scattering event (Fig. 1c). As a result, the electron–lattice cooling can be slow for phonon temperatures $T_{ph} \gg T_{BG}$, requiring many scattering events to dissipate the heat of the hot electrons.

On the other hand, a recent theory predicts alternative cooling pathways mediated by supercollisions[4] (SCs). Here, disorder-assisted phonon scattering or two-phonon scattering events enable the emission of acoustic phonons with wave vectors $q \geq 2k_F$, thus transferring higher energy than normal collisions. Such collisions occur less frequently than ordinary collisions, but dominate the electron–lattice cooling by using the entire thermal distribution of phonons (Fig. 1c).

A unique feature of graphene is the tunability of T_{BG} with Fermi energy E_F (ref. 3). As both the electron and the phonon energy are linear in wave vector, the Bloch–Grüneisen temperature is simply given by $k_B T_{BG} = (2v_s/v_F)E_F$, where v_s and v_F are the sound and the Fermi velocity, respectively. Hence, both energy scales, $k_B T_{BG}$ and E_F, are linked by the ratio $2v_s/v_F \approx 0.04$.

In this work, we experimentally test the different models of electron–phonon cooling[4–8]. The low- ($T_{ph} < T_{BG}$) and high-temperature ($T_{ph} > T_{BG}$) regimes become accessible by tuning the size of the Fermi surface, that is tuning T_{BG} by means of an electrostatic gate potential V_g (Fig. 1). Electrons are heated with a bias voltage V in a two-probe configuration, and the electron–lattice cooling rate is investigated by means of Johnson noise thermometry, a primary temperature measurement technique based on the fundamental properties of thermal fluctuations in conductors. The electron temperature is deduced from radio frequency Johnson noise measurements, relying on the relation $S_I = 4k_B T_e/R$ between the current noise spectrum S_I, the sample resistance R, and T_e. Johnson-noise thermometry has proven useful to study carbon nanotubes[9,10] and more recently graphene[11,12]. In the high-temperature regime $T_{ph} \geq T_{BG}$, we find an energy relaxation rate, $J_{SC} = A(T_e^3 - T_{ph}^3)$, as predicted by the supercollision mechanism[4], with a prefactor A related to the amount of disorder and the carrier density. Uniquely in graphene, there is a regime where disorder-assisted SCs dominate over the conventional electron–phonon collisions[5–8] above T_{BG}. In the low-temperature regime, for $T_{ph} < T_{BG}$, we regain the dependence $J \propto (T_e^4 - T_{ph}^4)$ (refs 7,8,12,13), which is the signature of standard electron–phonon interaction in 2D graphene.

Figure 2 shows the increase of electron temperature as a function of dissipated Joule power in a monolayer graphene device on a hexagonal boron nitride (h-BN) substrate. The average electron temperature T_e is extracted from the noise S_I, measured in the megahertz to gigahertz band to overcome the environmental $1/f$ contribution (see Methods). With the application of the Joule power P to the electron system, T_e rises well above the substrate temperature $T_0 = 4.2$ K: T_e reaches 300–700 K when $\sim$1 mW of Joule power is generated in our $\sim 5\,\mu m^2$ sized sample. The large increase of T_e is partly due to the much smaller carrier density in graphene compared to a conventional metal. The Joule power is dissipated in a relatively small number of carriers, resulting in the corresponding increase of T_e. Accordingly, we find T_e to be at its largest value at the charge neutrality point (CNP), located at $V_g = 12$ V (inset of Fig. 2). Moving away from the CNP (that is, increasing the carrier density n_s) T_e decreases at constant power P.

The large thermal decoupling of electrons and phonons ($T_e \gg T_{ph} \gtrsim T_0$) reflects the weak electron–phonon interaction

[1]Laboratoire Pierre Aigrain, ENS-CNRS UMR 8551, Universités P. et M., Curie and Paris-Diderot, 24 rue Lhomond, 75231 Paris Cedex 05, France, [2]Laboratoire de Photonique et Nanostructures, CNRS-UPR20 CNRS, Route de Nozay, 91460 Marcoussis Cedex, France. †These authors contributed equally to this work. *e-mail: bernard.placais@lpa.ens.fr.

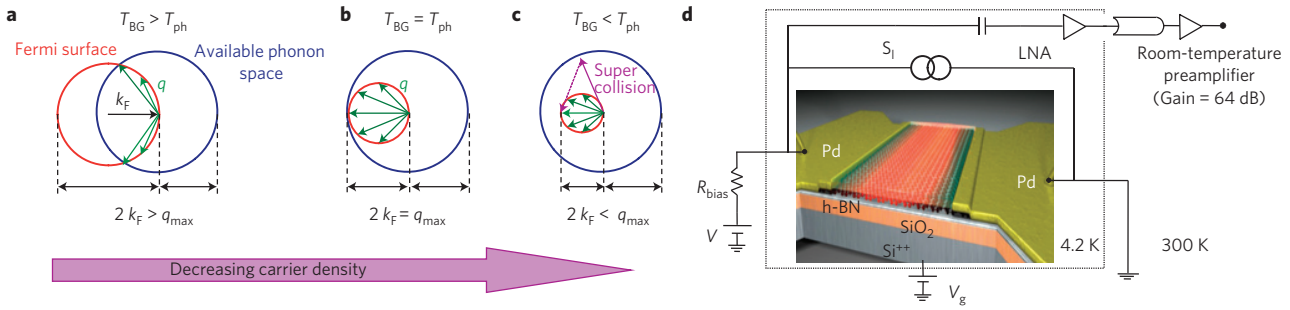

Figure 1 | Tunability of the Bloch–Grüneisen temperature and noise thermometry set-up. a, Electron–phonon interactions scatter carriers from one point on the Fermi surface (red circle) to another, within the boundary of the available phonon space (blue circle). In low-temperature regime ($T_{ph} < T_{BG}$), q_{max} is smaller than $2k_F$, which represents a full backscattering of electrons. **b**, The Fermi surface shrinks as the carrier density decreases, resulting in a smaller value of T_{BG}. Here, when $T_{ph} = T_{BG}$, q_{max} just equals $2k_F$. **c**, In the vicinity of the charge neutrality point, one enters the high-temperature regime, where $T_{ph} > T_{BG}$. Here, only phonons with $q \leq 2k_F$ can scatter off the electrons in the ordinary collisions (green arrows), whereas the entire thermal distribution of phonons is allowed for disorder-assisted supercollisions (purple arrow). **d**, Sketch of noise thermometry set-up. Measurements are carried out in liquid helium immersion: Joule power is supplied to the sample, creating a hot-carrier population. The hot electrons (diffuse red) induce a thermal noise (current generator S_I) and are cooled by the graphene lattice (small balls). The current fluctuations are amplified using a cryogenic low-noise amplifier (LNA).

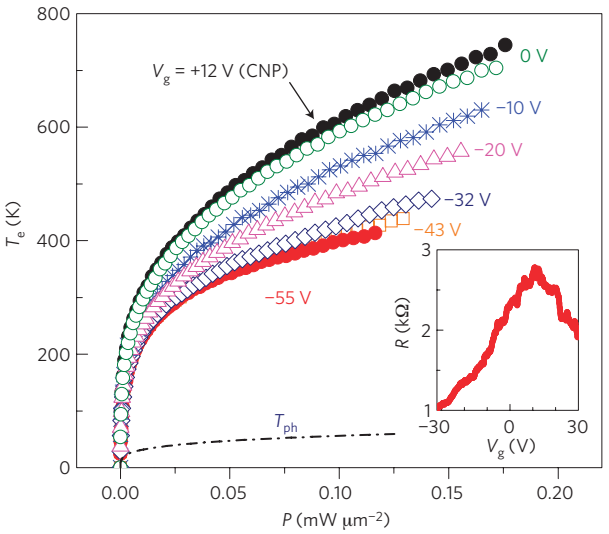

Figure 2 | Electron temperature in graphene as a function of supplied Joule power. Electron temperature as a function of Joule power per unit area, $P = V^2/(RWL)$, in a sample of width $W = 2.8\,\mu m$ and length $L = 2.2\,\mu m$. Data is shown for selected gate voltages: V_g ranges from high carrier density (−55 V) to charge neutrality ($V_g = 12$ V). For comparison, the lattice temperature (dashed line) is estimated from $T_{ph} \approx (P/\Sigma_K)^{1/4}$ with the lattice-substrate coupling constant $\Sigma_K \simeq 10\,Wm^{-2}K^{-4}$. Inset: Resistance as a function of gate voltage at 4.2 K.

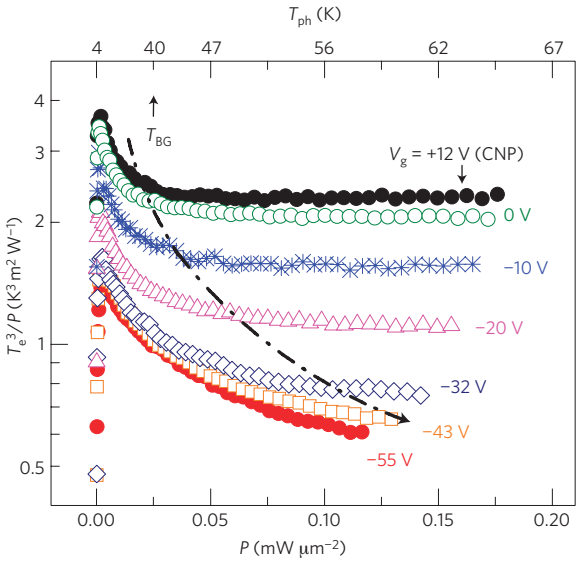

Figure 3 | Supercollision cubic law. Electron temperatures are plotted as T_e^3/P for a range of selected gate voltages. T_{BG} is tuned by the electrostatic gate potential, and shown as the dashed-dotted line. For temperatures $T_{ph} > T_{BG}$, the SC cooling dominates, visible from the arising plateaux in the T_e^3/P representation.

in graphene. The steady-state value of T_e is determined by the balance between the Joule heating P and the cooling power J at play[14]. The cooling of electrons occurs either through heat transfer to the phonons or heat diffusion to the metallic leads. The heat diffusion length, inversely proportional to T_e, is typically ∼250 nm at $T_e = 400$ K, which is one tenth of the sample length. Therefore, at sufficiently high bias ($P \gtrsim 10\,\mu W\,\mu m^{-2}$) the diffusive contribution can be neglected, and the electron–lattice cooling can be directly investigated[12]. Similarly, T_{ph} reaches a steady-state value when the same power from the electrons is transferred to the substrate with a typical black-body radiation law $P = \Sigma_K(T_{ph}^4 - T_0^4)$. The phonon–substrate coupling constant[15], $\Sigma_K \simeq 10\,Wm^{-2}K^{-4}$, is 3–4 orders of magnitude larger than the electron–phonon coupling constant in graphene[12], and we achieve phonon temperatures $T_{ph} \simeq 4$–65 K with $P = 0$–$0.2\,mW\,\mu m^{-2}$.

To test the supercollision mechanism, we plot in Fig. 3 the electron temperature in the representation T_e^3/P as a function of P. SC theory predicts the energy loss power

$$J_{SC} = A\,(T_e^3 - T_{ph}^3), \quad A = 9.62\,\frac{g^2\nu^2(E_F)k_B^3}{\hbar k_F l} \qquad (1)$$

while modelling disorder by short-range scatterers. Here g is the electron–phonon coupling, $\nu(E_F)$ is the density of states per spin/valley flavour, and l is the mean free path. In this model $k_F l$ is a constant inversely proportional to the strength and concentration of impurities. Other types of disorder, such as ripples[4] or to some extent long-range impurities can give rise to a similar T^3 dependence; however, with different expressions for the coupling constant. Note that, with $T_e \gg T_{ph}$, the T_e^3/P plateau corresponds to the inverse of the coupling constant A.

The T_e^3/P plots (Fig. 3) demonstrate three different cooling regimes; the dip at $P \approx 0$ representing the heat conduction to

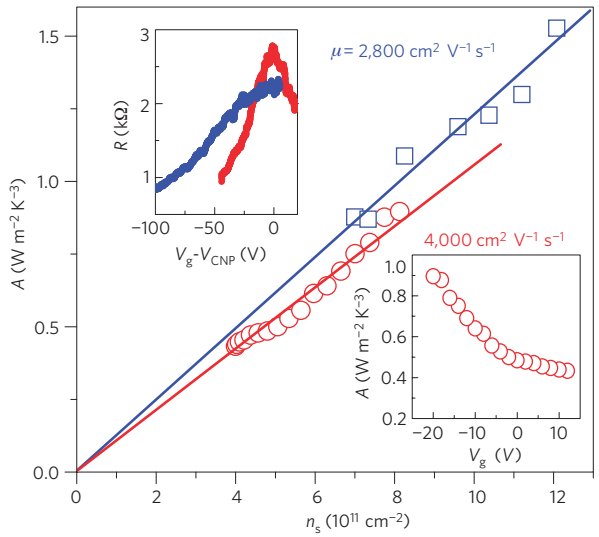

Figure 4 | SC coupling constant *A* as a function of carrier density. The coupling constant *A* increases linearly with the carrier density and is dependent on the level of disorder in the sample. The latter is changed by a heat treatment: red circles and blue squares correspond to data acquired before and after annealing, respectively. Right inset: Coupling constant *A* as a function of gate voltage, deduced from the T_e^3/P plateaux for steps of 2 V in the range $-20\,\mathrm{V} \le V_g \le 12\,\mathrm{V}$. Left inset: Resistance versus $(V_g - V_{CNP})$ measured at 4.2 K before (red) and after (blue) the heat treatment.

the leads, the asymptotic $P \propto T_e^3$ behaviour (the T_e^3/P plateau) pronounced in the high-temperature regime ($T_{ph} > T_{BG}$), and the low-temperature $P \propto T_e^4$ behaviour[12] at $T_{ph} < T_{BG}$, which translates into a decreasing function $T_e^3/P \sim P^{-1/4}$. To highlight the border between the low- and high-temperature regimes, the gate-tuned T_{BG} is visualized by a dashed–dotted line which connects the values of T_{BG} at each V_g, while T_{ph} is denoted in the upper x axis of the Fig. 3. We use the relation $T_{BG} = (2v_s/v_F)E_F/k_B \approx 54\sqrt{n_s}$ K, where the carrier density $n_s = \sqrt{[C_g(V_g - V_{CNP})/e]^2 + n_0^2}$ (in units of $10^{12}\,\mathrm{cm}^{-2}$) is deduced from the gate voltage V_g using the gate capacitance $C_g = 35\,\mathrm{aF\,\mu m}^{-2}$ (e is the elementary charge). C_g is estimated from device geometry. We have introduced a residual density $n_0 \simeq 4 \times 10^{11}\,\mathrm{cm}^{-2}$ to account for the minimum conductivity due to electron–hole puddles at the CNP.

Our observation of the T_e^3/P plateaux, which are most pronounced near the charge neutrality point, strongly supports the SC cooling mechanism in the high-temperature regime. With increasing n_s (resp. $T_{BG} \propto \sqrt{n_s}$), plateaux start to develop at larger P (resp. T_{ph}), up to a point where the low-temperature regime ($T_{ph} < T_{BG}$) dominates over the entire power range (for $V_g \lesssim -32$ V).

We now focus on the high-temperature regime and compare in greater detail the SC theory to our data. The short-range disorder-assisted SCs, shown in equation (1), scale linearly with carrier density, $n_s \sim v^2(E_F)$. In Fig. 4, the SC coupling constant A, extracted from the T_e^3/P plateau, is presented for $-20\,\mathrm{V} \le V_g \le 12\,\mathrm{V}$ (red dots). Indeed, we find a linear dependence $A \propto n_s$, in good agreement with the SC theory. Evaluating equation (1), we obtain $A \approx 7.5 \times 10^{-4}\ (D^2 n_s/k_F l)\,(\mathrm{W}/(\mathrm{m}^2\mathrm{K}^3))$, where D is the deformation potential in eV, and n_s in units of $10^{12}\,\mathrm{cm}^{-2}$. Taking $k_F l = \sigma(h/2e^2) \approx 3.5$, from conductivity data, the slope in Fig. 4 indicates a deformation potential $D \approx 70$ eV, larger than the reported values $D \sim 10$–30 eV (refs 3,16,17). We are led to the conclusion that, although equation (1) gives the order of magnitude, correct carrier density, and temperature dependence of the cooling power, it also leads to an underestimate of the coupling constant. This is possibly an indication that the short-range scattering hypothesis is too restrictive.

To check the disorder dependence in A, we have increased the impurity content of the sample by a heat treatment; this has shifted the CNP to 115 V, and decreased the mobility accordingly (see left inset of Fig. 4). Consistently we observe a ∼30% increase of the coupling constant (blue squares in Fig. 4), which confirms the effect of impurity concentration as predicted in equation (1).

Turning to the discussion of the results, the enhancement factor for the disorder-assisted SC cooling over the conventional cooling pathways, $J_0 \propto (T_e - T_{ph})$, is given as in ref. 4

$$\frac{J_{SC}}{J_0} = \frac{0.77}{k_F l}\,\frac{T_e^2 + T_e T_{ph} + T_{ph}^2}{T_{BG}^2} \qquad (2)$$

At the CNP, we have $T_e \approx 400$ K and $T_{ph} \sim T_{BG} \approx 40$ K for $P = 0.025\,\mathrm{mW\,\mu m}^{-2}$ (Figs 2, 3). The enhancement factor J_{SC}/J_0 is as great as 80, and explains the immediate observation of the SC cubic law right above T_{BG}. Note that with a further increase of P (T_e and T_{ph}), the enhancement factor becomes even larger.

Although the cubic behaviour for SC and the linear law for normal collisions are valid in the degenerate limit, $k_B T_e < E_F$, the normal electron–phonon collisions are predicted to give $J \propto T_e^4\,(T_e - T_{ph})$ for $k_B T_e \gg E_F$ (refs 5,8). Proportional to T_e^5 (at $T_e \gg T_{ph}$), it might be possible for normal collisions to dominate again in the non-degenerate limit when T_e is sufficiently large. In our experiment, the residual carrier density at the CNP limits E_F above 65 meV, and we could not achieve the regime $k_B T_e \gg E_F$. Higher mobility samples are needed to access this non-degenerate regime, as well as electron cooling by optical phonons, which are both of great interest.

Also, we note that the proper choice of the substrate can be important in our study. SiO_2 substrates have a small surface optical phonon energy of 59 meV, and the coupling with substrate phonons can play an important role in cooling above several hundreds K[18,19]. The h-BN substrate used in our experiment has a much larger surface optical phonon energy of 102 meV (∼1,180 K; ref. 18). Therefore, the surface optical phonons of h-BN, as well as the optical phonons of graphene, may intervene at higher temperatures, but they can be disregarded in our experiment, where $T_e \lesssim 700$ K.

In conclusion, we have investigated the impurity-mediated electron–phonon interaction in diffusive graphene by measuring the energy loss of hot electrons both below and above the Bloch–Grüneisen temperature for phonons. We observe the T_e^3 dependence on the electronic temperature predicted for supercollisions at high temperature while recovering the T_e^4 dependence for ordinary collisions at low temperature. The Bloch–Grüneisen crossover temperature agrees with the estimated phonon temperature and the coupling constant is consistent with the carrier density and disorder dependence predicted for short-range impurity scattering. Beside its implication for electron–phonon physics, our work is of direct relevance for the performance of graphene bolometers and photo-detectors[20–23].

During the writing of this manuscript, we have become aware of a preprint[24] dealing with SC cooling in graphene. In this experiment the photocurrent generated at a graphene p–n junction is described well by the SC cubic law.

Methods

The experiments were performed on exfoliated monolayer graphene on h-BN/SiO_2/Si substrates. The h-BN platelet was exfoliated from a high-quality h-BN powder (St Gobain 'Très BN'.) The graphene flake was subsequently placed on top of the h-BN using a transfer technique described in ref. 25. The heavily p-doped Si was used as a back gate and the thickness of the insulating layer was ∼1 μm. The samples, produced by means of e-beam lithography and dry etching, were embedded in a coplanar waveguide adapted for GHz frequencies[26].

We applied a Joule power $P = V^2/R$ to create the hot-carrier population and study the electronic cooling, as shown in Figs 2 and 3. The sample's length and width

were $L = 2.2\,\mu$m and $W = 2.8\,\mu$m, respectively. The sample resistance $R \sim 1/n_s$ was calculated from the voltage drop across the bias resistance $R_{\rm bias} = 4.7\,{\rm k}\Omega$ (see Fig. 1d). The carrier density n_s was controlled electrostatically by means of the back-gate voltage $V_{\rm g}$.

All data was measured for samples in a direct contact with liquid helium to ensure a cold phonon bath. The noise signal resulting from the hot carriers was first amplified by a cryogenic low-noise amplifier at $T = 4.2$ K followed by two additional amplifiers at room temperature (overall gain of ≈ 82 dB). A 460 Ω $Al/AlO_x/Al$ tunnel junction was used to calibrate the shot noise. Our broadband set-up, with a bandwidth of ∼1 GHz, allows us to quantitatively separate the white noise contribution S_I from $1/f$ noise by fitting the spectra with a $S_I + C/f$ law. We find $C \propto I^2$, in accordance with the Hooge law[27]. This procedure is especially important for small samples and high currents, where the $1/f$ contribution can be large.

Received 17 August 2012; accepted 26 October 2012; published online 2 December 2012

References

1. Castro Neto, A. H., Guinea, F., Peres, N. M. R., Novoselov, K. S. & Geim, A. K. The electronic properties of graphene. *Rev. Mod. Phys.* **81,** 109–162 (2009).
2. Das Sarma, S., Adam, S., Hwang, E. H. & Rossi, E. Electronic transport in two dimensional graphene. *Rev. Mod. Phys.* **83,** 407–470 (2012).
3. Efetov, D. K. & Kim, P. Controlling electron–phonon interactions in graphene at ultrahigh carrier densities. *Phys. Rev. Lett.* **105,** 256805 (2010).
4. Song, J. C. W., Reizer, M. Y. & Levitov, L. S. Disorder-assisted electron–phonon scattering and cooling pathways in graphene. *Phys. Rev. Lett.* **109,** 106602 (2012).
5. Bistritzer, R. & MacDonald, A. H. Electronic cooling in graphene. *Phys. Rev. Lett.* **102,** 206410 (2009).
6. Tse, W-K. & Das Sarma, S. Energy relaxation of hot Dirac fermions in graphene. *Phys. Rev. B* **79,** 235406 (2009).
7. Kubakaddi, S. S. Interaction of massless Dirac electrons with acoustic phonons in graphene at low temperatures. *Phys. Rev. B* **79,** 075417 (2009).
8. Viljas, J. K. & Heikkilä, T. T. Electron–phonon heat transfer in monolayer and bilayer graphene. *Phys. Rev. B* **81,** 245404 (2010).
9. Chaste, J. *et al.* Thermal shot noise in top-gated single carbon nanotube field effect transistors. *Appl. Phys. Lett.* **96,** 192103 (2010).
10. Wu, F., Virtanen, P., Andresen, S., Plaçais, B. & Hakonen, P. J. Electron–phonon coupling in single-walled carbon nanotubes determined by shot noise. *Appl. Phys. Lett.* **97,** 262115 (2010).
11. Fay, A. & Tomi, *et al.* Shot noise and conductivity at high bias in bilayer graphene: Signatures of electron-optical phonon coupling. *Phys. Rev. B* **84,** 245427 (2011).
12. Betz, A. C. *et al.* Hot electron cooling by acoustic phonons in graphene. *Phys. Rev. Lett.* **109,** 056805 (2012).
13. Baker, A. M. R, Alexander-Webber, J. A., Altebaeumer, T. & Nicholas, R. J. Energy relaxation for hot Dirac fermions in graphene and breakdown of the quantum Hall effect. *Phys. Rev. B* **85,** 115403 (2012).
14. Wellstood, F. C., Urbina, C. & Clarke, J. Hot-electron effects in metals. *Phys. Rev. B* **49,** 5942–5955 (1994).
15. Balandin, A. A. Thermal properties of graphene and nanostructured carbon materials. *Nature Mater.* **10,** 569–581 (2011).
16. Bolotin, K. I., Sikes, K. J., Hone, J., Stormer, H. L. & Kim, P. Temperature-dependent transport in suspended graphene. *Phys. Rev. Lett.* **101,** 096802 (2008).
17. Dean, C. R. *et al.* Boron nitride substrates for high-quality graphene electronics. *Nature Nanotech.* **5,** 722–726 (2010).
18. Low, T., Perebeinos, V., Kim, R., Freitag, M. & Avouris, P. Cooling of photoexcited carriers in graphene by internal and substrate phonons. *Phys. Rev. B* **86,** 045413 (2012).
19. Price, A. S., Hornett, S. M., Shytov, A. V., Hendry, E. & Horsell, D. W. Nonlinear resistivity and heat dissipation in monolayer graphene. *Phys. Rev. B* **85,** 161411 (2012).
20. Gabor, N. M. *et al.* Hot carrier assisted intrinsic photoresponse in graphene. *Science* **334,** 648–652 (2011).
21. Vora, H., Kumaravadivel, P., Nielsen, B. & Du, X. Bolometric response in graphene based superconducting tunnel junctions. *Appl. Phys. Lett.* **100,** 153507 (2012).
22. Yan, J. *et al.* Dual-gated bilayer graphene hot-electron bolometer. *Nature Nanotech.* **7,** 472–478 (2012).
23. Fong, K. C. & Schwab, K. C. Ultrasensitive and wide-bandwidth thermal measurements of graphene at low temperatures. *Phys. Rev. X* **2,** 031006 (2012).
24. Graham, M. W., Shi, S-F., Ralph, D. C., Park, J. & McEuen, P. L. Photocurrent measurements of supercollision cooling in graphene. *Nature Phys.* http://dx.doi.org/10.1038/nphys2493 (2012).
25. Schneider, G. F., Calado, V. E., Zandbergen, H., Vandersypen, L. M. K. & Dekker, C. Wedging transfer of nanostructures. *Nano Lett.* **10,** 1912–1916 (2010).
26. Pallecchi, E. *et al.* Graphene microwave transistors on sapphire substrate. *Appl. Phys. Lett.* **99,** 113502 (2011).
27. Hooge, F. N., Kleinpenning, T. G. M. & Vandamme, L. K. J. Experimental studies on 1/f noise. *Rep. Prog. Phys.* **44,** 479–532 (1981).

Acknowledgements

The research has been supported by the contracts ANR-2010-BLAN-MIGRAQUEL, SBPC and Cnano-2011 Topin's and Grav's.

Author contributions

A.C.B. and S.H.J. conducted the noise measurements; R.F. performed the calculations of the supercollisions; E.P. participated in the early stage of the experiment. G.F. and J-M.B. supported the experiments; S.H.J. and B.P. wrote the paper; and B.P. initiated the experiment.

Additional information

Reprints and permissions information is available online at www.nature.com/reprints. Correspondence and requests for materials should be addressed to B.P.

Competing financial interests

The authors declare no competing financial interests.